Leveraging RALI-THINICE Observations to Assess How the ICOLMDZ Model Simulates Clouds Embedded in Arctic Cyclones

Lea Raillard, Étienne Vignon, Gwendal Rivière, Jean-baptiste Madeleine, Yann Meurdesoif, Julien Delanoë, Arnaud Caubel, Olivier Jourdan, Antoine Baudoux, Sébastien Fromang, et al.

JGR Atmospheres

RESEARCH ARTICLE
10.1029/2024JD040973

Leveraging RALI-THINICE Observations to Assess How the ICOLMDZ Model Simulates Clouds Embedded in Arctic Cyclones

Lea Raillard[1], Étienne Vignon[1], Gwendal Rivière[1], Jean-Baptiste Madeleine[1], Yann Meurdesoif[2], Julien Delanoë[3], Arnaud Caubel[2], Olivier Jourdan[4], Antoine Baudoux[4], Sébastien Fromang[2], and Philippe Conesa[2]

[1]Laboratoire de Météorologie Dynamique-IPSL, Sorbonne Université/CNRS/Ecole Normale Supérieure-PSL Université/Ecole Polytechnique-Institut Polytechnique de Paris, Paris, France, [2]Laboratoire des Sciences du Climat et de l'Environnement, LSCE/IPSL, CEA-CNRS-UVSQ, Université Paris-Saclay, Gif-sur-Yvette, France, [3]Laboratoire Atmosphère, Milieux et Observations Spatiales, LATMOS/IPSL, UVSQ Université Paris-Saclay, Sorbonne Université, CNRS, Guyancourt, France, [4]Laboratoire de Météorologie Physique, Université Clermont Auvergne/OPGC/CNRS, Clermont-Ferrand, France

Key Points:

- Airborne RALI-THINICE observations are used to evaluate Arctic clouds in the new limited area version of the ICOLMDZ model
- A methodology has been developed to make robust and co-located model-observation comparisons
- ICOLMDZ simulates overly high amounts of liquid and ice in clouds particularly near cloud top

Correspondence to:

L. Raillard,
lea.raillard@lmd.ipsl.fr

Citation:

Raillard, L., Vignon, É., Rivière, G., Madeleine, J.-B., Meurdesoif, Y., Delanoë, J., et al. (2024). Leveraging RALI-THINICE observations to assess how the ICOLMDZ model simulates clouds embedded in Arctic cyclones. *Journal of Geophysical Research: Atmospheres*, *129*, e2024JD040973. https://doi.org/10.1029/2024JD040973

Received 8 FEB 2024
Accepted 30 JUL 2024

Abstract Despite their essential role in the high-latitude climate, the representation of mixed-phase clouds is still a challenge for Global Climate Models (GCMs)'s cloud schemes. In this study we propose a methodology for robustly assessing Arctic mixed-phase cloud properties in a climate model using airborne measurements. We leverage data collected during the RALI-THINICE airborne campaign that took place near Svalbard in August 2022 to evaluate the simulation of mid-level clouds associated with Arctic cyclones. Simulations are carried out with the new limited-area configuration of the ICOLMDZ model which combines the recent icosahedral dynamical core DYNAMICO and the physics of LMDZ, the atmospheric component of the IPSL-CM Earth System Model. Airborne radar and microphysical probes measurements are then used to evaluate the simulated clouds. A comparison method has been set-up to guarantee as much as possible the spatiotemporal co-location between observed and simulated cloud fields. We mostly focus on the representation of ice and liquid in-cloud contents and on their vertical distribution. Results show that the model overestimates the amount of cloud condensates and exhibits a poor cloud phase spatial distribution, with too much liquid water far from cloud top and too much ice close to it. The downward gradual increase in snowfall flux is also not captured by the model. This in-depth model evaluation thereby pinpoints priorities for further improvements in the ICOLMDZ cloud scheme.

Plain Language Summary Mixed-phase clouds, where ice crystals and supercooled liquid droplets coexist at sub-zero temperatures, are ubiquitous in the polar regions. Albeit essential for the high-latitude climate, they are still poorly represented by climate models. In this study, original measurements from the RALI-THINICE airborne campaign, which took place in the Svalbard region in August 2022, are used to assess how the ICOLMDZ atmospheric model represents Arctic mixed phase clouds. A methodology is developed to make robust and co-located model-aircraft observation comparisons. In situ cloud probes and onboard radars are then used to evaluate the simulated amounts of liquid water and ice in clouds as well as the snowfall flux in deep clouds associated with the transit of Arctic cyclones. The results of the model evaluation show an overall overestimation of cloud condensates with too much liquid water far from cloud top and too much ice close to it.

1. Introduction

Mixed phase clouds (MPCs) are ubiquitous over the whole Arctic region and are present in all seasons, in particular in the Svalbard region (Mioche et al., 2015). MPCs are a key component of the Arctic climate (Kay et al., 2016) at least for two reasons. First, as MPCs are generally precipitating clouds (Silber et al., 2021), they play an important role in the Arctic water cycle and are the main source of water for the Greenland ice sheet (J. Lenaerts et al., 2020; McIlhattan et al., 2017). Second, the MPC radiative forcing is of first-order importance for the surface radiative budget over the Arctic Ocean and sea-ice—particularly during the fall season (e.g., Kay & Gettelman, 2009; Kay et al., 2016)—as well as for the surface melt of the Greenland ice sheet (Hofer et al., 2019). The MPC radiative effect is strongly determined by the amount of supercooled liquid water in clouds, mostly because liquid droplets enhance cloud optical depth and emissivity.

A correct representation of MPCs in atmospheric models is therefore essential to properly simulate the present and future of the Arctic climate. However, the modeling of MPCs in atmospheric models is a long-standing challenge (Klein et al., 2009; Morrison et al., 2012). Global Climate Models (GCMs) particularly struggle in representing the correct amount of supercooled liquid water, the phase partitioning and the precipitation production in these clouds (Cesana et al., 2015; Komurcu et al., 2014; J. T. Lenaerts et al., 2017; McCusker et al., 2023; Rotstayn et al., 2000). In particular, commonly used temperature dependent phase-partitioning functions have been shown to be inappropriate to simulate polar MPCs (Forbes & Ahlgrimm, 2014). The complexity of representing mixed phase clouds lies partly in the difference in scales between microphysical processes and the resolution of climate model grid-boxes (both horizontal and vertical) (A. I. Barrett et al., 2017; Forbes & Ahlgrimm, 2014; Korolev & Milbrandt, 2022), and partly in the complex interplay between aerosols, ice crystals and droplets microphysics, turbulent motions and large-scale dynamics which challenge the state-of-the-art parameterizations of clouds and turbulence (P. A. Barrett et al., 2020; Furtado et al., 2016; Morrison et al., 2009; Vignon et al., 2021).

To improve our understanding of the physical processes governing the physics of MPCs and to guide their parameterization in models, observations have been shown to be particularly helpful (Fridlind & Ackerman, 2018).

Satellite active remote sensing observations from the Cloud Profiling Radar aboard Cloudsat and from the CALIOP lidar aboard CALIPSO have been used to evaluate the representation of polar clouds—among which MPCs—in climate models and atmospheric reanalyses (J. T. Lenaerts et al., 2017). However, those data have non-negligible intrinsic limits. They do not give access to the in-cloud liquid water content below the attenuation layer of the lidar (often the uppermost supercooled liquid layer); radar data are contaminated by ground-clutter below about 1 km a.g.l. and the liquid and ice water content retrievals from the radar reflectivity and lidar back-scattering signal strongly depend on microphysical assumptions. Albeit spatially and temporally more limited, remote sensing and in situ measurements from airborne field campaigns give a more direct access to the local structure and properties of clouds.

In the past 20 years, an increasing number of airborne campaigns have focused on Arctic clouds. Boundary layer clouds, which dominate the total cloud coverage and the surface energy budget in the Arctic (Morrison et al., 2012) have been the target of several airborne field campaigns, for example, M-PACE (2004, Verlinde et al., 2007), ACLOUD (2017, Wendisch et al., 2019), Mosaic-ACA (2020, Shupe et al., 2022) and associated model evaluation exercises (e.g., Klein et al., 2009). Mid-level and deep Arctic clouds have been sampled occasionally during campaigns (e.g., during ACLOUD) but their characterization and representation in large-scale models have received less attention hitherto despite their important contribution to precipitation production (Lackner et al., 2023). They had further not been the proper focus of any dedicated campaign before THINICE, which occurred in the Svalbard region in August 2022. THINICE was dedicated to studying summertime Arctic cyclones and their interactions with tropopause polar vortices, clouds and sea ice.

The THINICE component related to the flights of the ATR42 aircraft operated by SAFIRE, the French facility for airborne research, was called RALI-THINICE and was more specifically dedicated to studying interactions between Arctic cyclones and clouds. A particular focus was given on the microphysics of mid-level mixed phase clouds whose formation is driven by the dynamics of cyclones but which also feedback on the dynamics itself through diabatic effects. Airborne in situ measurements of cloud properties as well as measurements from airborne radars and lidars have been collected.

Airborne in situ and remote sensing data can be extremely valuable to carry out climate models' evaluation in terms of wind and temperature in Arctic cyclones but more importantly in terms of liquid and ice water contents in mid-level polar MPCs (e.g., Listowski & Lachlan-Cope, 2017).

Nonetheless, the spatio-temporal resolution of observations is very different from that of atmospheric models. Simulated clouds do not necessarily coincide—in time and space—with those observed and the microphysical variability sampled in observations is often not represented—or parameterized—in models. Drawing reliable and useful conclusions on model performances thus requires thinking and developing a robust methodology of observation-simulation comparison.

The objective of the present paper is to leverage the RALI-THINICE cloud observations in order to properly and reliably evaluate the properties of mid-level and deep Arctic clouds as simulated by the ICOLMDZ model. We

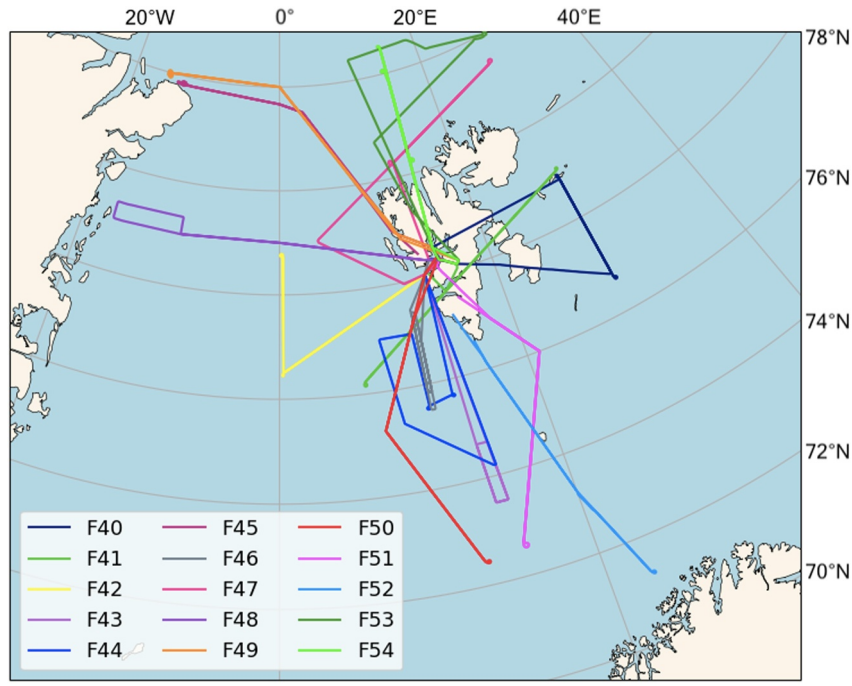

Figure 1. Trajectory of 15 flights of the Safire ATR42 aircraft made during RALI-THINICE (5–26 August 2022) whose measurements are used in this study.

will apply our methodology to simulations performed with the ICOLMDZ model, which is a new combination of the physics of the LMDZ model (Hourdin et al., 2020), the atmospheric component of the IPSL Climate Model (Boucher et al., 2020), with the icosahedral dynamical fluid solver DYNAMICO (Dubos et al., 2015). It is worth noting that the improvement of polar clouds have been identified as a development priority for LMDZ after the sixth exercise of the Couple Model Intercomparison Project (CMIP6, Madeleine et al., 2020) since their parameterization remains quite coarse and has been poorly evaluated so far. The manuscript is structured as follows. Section 2 details the instrumentation, the main features of ICOLMDZ and the simulations set up. The comparison methodology is described in Section 3. The results are presented in Section 4 with first, an illustration of the methodology on a case study of a single flight and second, a statistical analysis based on all flights of the campaign. Section 5 closes the paper with a summary and a conclusion.

2. Data and Model

2.1. Observations

2.1.1. The RALI-THINICE Campaign

The data used in this study are based on measurements collected in August 2022 near the Svalbard archipelago with the ATR42 research aircraft operated by SAFIRE (http://www.safire.fr), the French facility for airborne research, as part of the RALI-THINICE campaign. During the campaign, the ATR42 was based in Longyearbyen (78.23°N, 14.90°E, Svalbard, Norway) and sampled four cases of summer cyclones during a total of 16 flights, to characterize the dynamical structure of summertime Arctic cyclones and the microphysical properties of the associated clouds. The trajectories of the 15 flights used in the present study are plotted in Figure 1. It includes all the scientific flights, except flight numbered 39 which was a test flight.

2.1.2. In Situ Microphysical Measurements

Cloud microphysical and optical properties have been measured with a set of 5 probes from the French Airborne Measurement Platform. In this study, we use measurements collected by three instruments: the Cloud Droplet Probe (CDP-2), the 2 Dimensions Stereo imager (2D-S) and the High Volume Precipitation Spectrometer (HVPS).

The Cloud Droplet Probe (CDP-2, Lance et al., 2010) equipped with anti-shattering tips is a forward scattering optical size spectrometer of individual water droplets with size ranging from 2 to 50 μm. Droplet particle size distributions on 30 bins with variable widths (1–2 μm) are derived from this instrument. The 2D Stereo imaging Probe (2DS, Lawson et al., 2006) and the High Volume Precipitation Spectrometer (HVPS, Lawson et al., 1993) are Optical Array Probes (OAP) that record two dimensional images of the shadow cast by hydrometeors on a 128 diode array with a 10 and 150 μm pixel resolution respectively. From these two OAPs, Particle size Distributions (PSDs) of water droplets and ice crystals on 125 size bins from 50 to 1,280 μm or 600–19 mm can be determined. The discrimination between liquid water droplets and ice crystals is performed based on the circularity of the sampled cloud particles (following Crosier et al. (2011)) supported by visual inspection of hydrometeor images. However this method is only valid for images corresponding to cloud particles with a surface larger than 16 pixels (i.e., hydrometeor with size larger than 100 μm for the 2DS). The total liquid water content (LWC) of water droplet with diameter ranging from 2 to 500 μm is inferred from the combined PSD measured by the CDP-2 and the 2D-S assuming that droplets are spherical. The total ice concentration size distribution is obtained by merging the 2DS ice size distribution from 50 to 675 μm with the HVPS PSD from 1,275 μm to 19 mm. To do so, a weighted averaging procedure is applied between 675 and 1275 μm where the two PSD overlap. The total ice water content (IWC) is then calculated using the modified Brown and Francis mass-maximum size relationship (Hogan et al., 2012).

2.1.3. Radar Measurements

The aircraft payload also comprised the multibeam 95 GHz Doppler spectral cloud radar RASTA (RAdar SysTem Airborne, Delanoë et al., 2013). Thanks to its three downward-looking and three upward-looking antennas we can retrieve the three-dimensional wind field (including the vertical velocity combination of the terminal fall velocity of the hydrometeors and the vertical air motion) below and above the aircraft after correcting for the aircraft motion.

A cloud mask is derived by removing the background noise of the radar signal for each antenna. This is a combination of a thresholding technique followed by an image processing approach in order to remove isolated pixels. Once the valid signal is identified the ground signal and artifacts are removed. The Doppler measurements are used to distinguish the cloud from precipitation. A melting layer detection is proposed by combining reflectivity and vertical velocity gradients.

The retrieval of the cloud IWC is based on a variational approach named Radonvar and built on earlier work by Delanoë et al. (2007) and Delanoë and Hogan (2008) using radar reflectivity and vertical velocity. The radar reflectivity is sensitive to the size and the concentration of the hydrometeors while the terminal fall velocity is dominated by the size, therefore such a combination allows us to constrain both size and concentration Delanoë et al. (2007, 2014). Snowfall flux is also estimated by multiplying the IWC retrieval with the retrieved vertical velocity.

Note that even though a lidar was also present onboard, the synergistic LWC retrieval is not considered here given that it was not available at the time of the study.

Figure 2 shows that a fair agreement is obtained when comparing radar and in situ probe IWC estimates during the full RALI-THINICE campaign. However, the RASTA retrieval tends to overestimate the high IWC values for which the retrieval is highly dependent upon the choice of the mass-diameter law. The mean relative difference between the two data sets $(IWC_{RASTA} - IWC_{\text{in situ}})/IWC_{\text{in situ}}$ is about 75%–100%.

2.2. Model, Configuration and Simulation Set Up

2.2.1. The ICOLMDZ GCM

The ICOLMDZ model consists in the recent coupling of the advanced DYNAMICO icosahedral dynamical core (Dubos et al., 2015) and the physics of LMDZ (Hourdin et al., 2020)—the atmospheric component of the IPSL Earth-System Model actively involved in the CMIP exercises (Boucher et al., 2020). In the present study, ICOLMDZ has been also coupled to Orchidee, the Land Surface component of the IPSL model (Cheruy et al., 2020). LMDZ has been traditionally used with a standard longitude-latitude dynamics and the present study is one of the first using simulations run with the ICOLMDZ configuration (see also Bourdin et al., 2023).

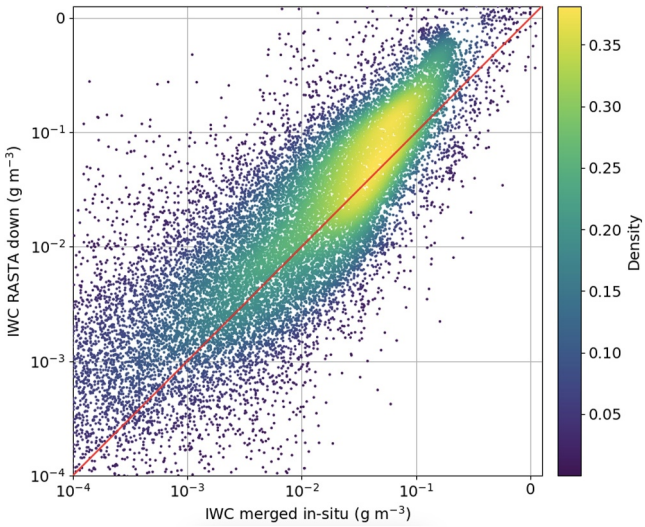

Figure 2. Scatter plot at the radar resolution, of the IWC in situ product and the IWC retrieval from RASTA for all the RALI-THINICE flights. Color shading indicates the density of points.

Clouds in LMDZ are parameterized using a statistical scheme assuming a subgrid distribution of total water from which the cloud fraction and condensates content within a grid cell are computed. A fixed monotonous temperature-dependent function is used to partition the cloud condensate variable into liquid and ice in the mixed-phase temperature regime.

The cloud parameterization is extensively described in Madeleine et al. (2020). We use in this study a version of the physics currently in development for CMIP7 that will be hereafter referred to as "CM7dev." In the latter, changes from the CMIP6 (Hourdin et al., 2020) version mostly consists in rewriting the cloud parameterization, including a new numerical treatment of the autoconversion process and activating a new parameterization for precipitation evaporation (Touzé-Peiffer, 2021) based on the work of Jakob and Klein (2000) in which rainfall and snowfall evaporate only in the cloud-free fraction of the mesh.

2.2.2. The Limited Area Model Configuration

As we want to properly capture the dynamical structure of Arctic cyclones as well as the induced meso-scale cloud heterogeneity, we want to run simulations with a resolution of the order of 20 km, which is quite challenging to achieve with standard GCMs. Moreover, to be able to perform several sensitivity numerical simulations, we need a simulation configuration computationally cheap.

All the simulations used in this work have therefore been performed with a new Limited Area Model (LAM) configuration of DYNAMICO. As the present paper is the first one using it, a short description of its characteristics is hereafter provided. The LAM horizontal grid is composed of 3 rhombus-shaped tiles defining an hexagonal domain. The domain is characterized by the position of its center and a radius value R and the horizontal resolution is set by dividing R with a prescribed number of hexagons (Figure 3). There are 3 distinct zones within the LAM domain. The outermost band of the hexagon (in red in Figure 3) is the raw forcing zone—with a fixed width of 5 grid cells—where lateral boundary conditions are applied at each dynamics time step that is, the value of the state variables of the model are prescribed with that of the forcing. Those lateral boundary conditions can be provided by either atmospheric reanalyses or climate model simulations. The innermost part (in white in Figure 3) is the free domain where the forcing is either no longer applied or applied through a nudging approach with a prescribed relaxation time τ_{in}. Between the raw forcing zone and the free domain, the transition zone of

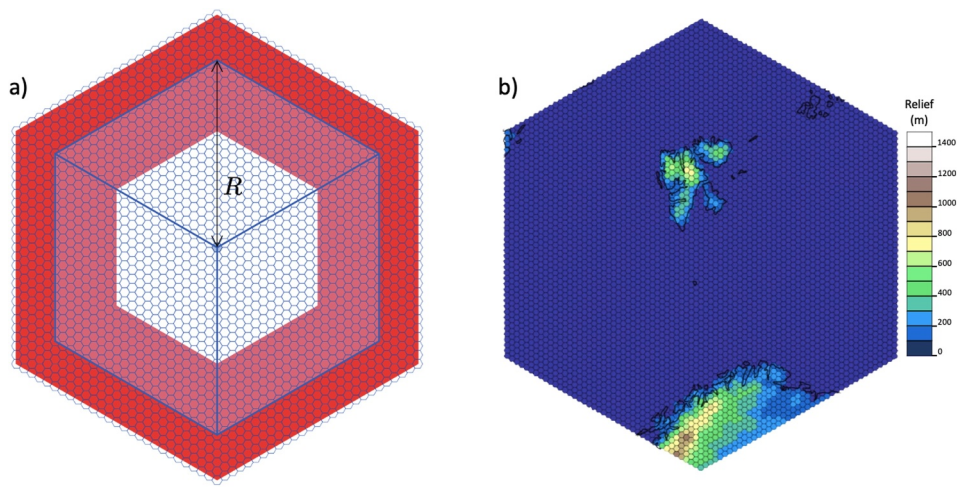

Figure 3. (a) Schematics of a LAM domain with the three zones: forcing zone (red), transition zone (light red), and free zone (white). Black arrow indicates the radius of the LAM. Blue lines delimit the 3 rhombus-shaped tiles defining the hexagonal domain. (b) Domain of simulation. Only the free and transition zones are shown.

adjustable thickness is where model state variables are nudged toward the forcing, the nudging timescale increasing—hence the nudging strength decreasing—with a hyperbolic tangent function between τ_{out} = 1hr by default, and τ_{in} toward the interior of the domain (Conesa, 2022).

2.2.3. Simulations Set-Up

The simulation domain chosen for this study is centered a 100 km south off the tip of Svalbard, at 76°N, 29°E (Figure 3). Lateral boundary conditions are computed from ERA5 hourly reanalyses (Hersbach et al., 2020). Sea ice concentration and sea surface temperature conditions are prescribed using ERA5 daily mean. With a radius of 1,100 km, subdivided into 40 hexagons, the horizontal resolution of our domain is 27.5 km. As stated above, to properly capture the cyclones structure, the clouds and the Svalbard topography, a fine resolution is needed, but the hydrostatic nature of the model as well as the physical hypotheses on which parameterizations are based prevent us from going below ≈20 km. We also want a resolution close to the forcing, that is, ≈30 km for ERA5 in our case. Attention has been paid not to cut the Greenland coastline, to avoid a steep change in topography at the edge of the domain. As most of the cyclones of the campaign were sampled before passing over the Svalbard, the clouds are not affected by the orography of the islands In the vertical direction, we use 95 hybrid-pressure levels with a resolution in the middle atmosphere ranging from about 150 m at 2,000–400 m at 7,000 m. A 7 months spin-up (January–July 2022) is run to properly initialize the soil moisture and snow cover on the Svalbard. We then ran a simulation for August 2022 (CM7dev). To improve the time and space colocation of the simulation with the aircraft measurements, we also ran a simulation (CM7dev-nudg) in which the wind is nudged inside the domain toward ERA5 with a relaxation time scale τ_{in} = 1 hr. Since the horizontal resolution of our model is close to that of ERA5, the small-scale features smoothing effect potentially induced by the nudging is very limited. Simulations' outputs are provided at an instantaneous hourly frequency and interpolated—with a conservative interpolation—onto a 1° × 0.25° longitude-latitude grid, which corresponds in the mid domain (76°N), to a spacing of 29 km × 27.5 km in longitude and latitude respectively.

3. Comparison Methodology

3.1. Cloud Definition

First, we want our model to properly simulate the correct mass of condensates within clouds, namely the in-cloud LWC and IWC. In the in situ observational data, clouds are distinguished from clear sky regions when the measured LWC and the measured IWC exceed arbitrary threshold values, in accordance with Moser et al. (2023) and Dupuy et al. (2018), that are: $LWC \geq 10^{-2}$ and $IWC \geq 10^{-4}$ g m^{-3}. These thresholds values have been determined empirically and correspond to the start of "jumps" in LWC and IWC time series coinciding to the time at which the aircraft enters a cloud.

In each grid cell of the model, the cloud parameterization computes a cloud fraction α_c, a clear-sky precipitation fraction α_{pr}^{cs} (corresponding respectively to blue and orange regions in Figure 4) as well as a specific amount of condensed water q_c and a precipitation flux for each phase for clear sky q_{pr}^{cs} and for cloud q_{pr}^{cld} (Touzé-Peiffer, 2021). The superscript *cs* and *cld* denotes respectively clear-sky and cloud quantities. The non-precipitating cloud condensates versus precipitation dichotomy in the model is purely arbitrary in the sense that it entirely depends on the way the autoconversion process is parameterized. Moreover, if separating cloud droplets from rain drops is somewhat physically reasonable as there is a clear separation in terms of size as well as in terms of growth mechanism—namely vapor diffusion for cloud droplets and collision-coalescence for rain drops—there is no clear limit between "cloud" ice crystals and those "precipitating." Thus distinguishing "cloud" condensates from "precipitating" ones in a common and robust way in both observations and in the model is very delicate, not to say impossible. Subsequently, the decision was made to compare for each phase the total water contents in the observation with the sum q_{eff} of both cloud q_c and precipitation q_{pr} water contents from the model. There are three different scenarios depending on whether the model grid cell is cloudy, contains precipitation but no cloud or is fully clear-sky (Figure 4):

$$q_{eff} = \begin{cases} \left(q_c + q_{pr}^{cld}\right)/\alpha_c & \text{if } \alpha_c \geq 0.1 \text{ (clouds)} \\ q_{pr}^{cs}/\alpha_{pr}^{cs} & \text{if } \alpha_c < 0.1 \text{ and } \alpha_{pr}^{cs} \geq 0.01 \text{ (precipitation zones)} \\ 0 & \text{else (clear-sky)} \end{cases}$$

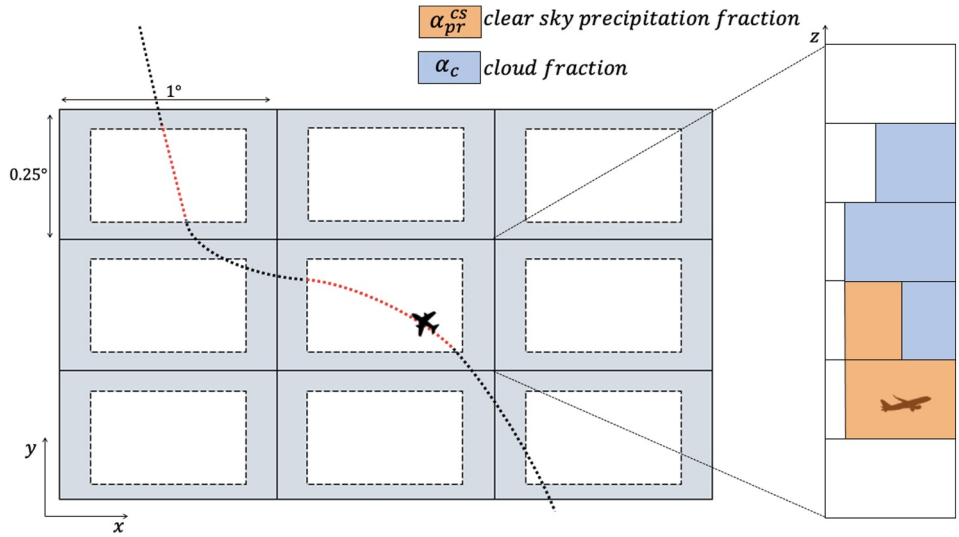

Figure 4. The left-hand side shows a schematic of the model's horizontal grid. The gray shading corresponds to the zone in which observations are discarded: only observations along the red part of the trajectory are kept for comparison. The right hand-side shows a schematic of a model column in which the cloud fraction is shown in blue and the clear-sky precipitation fraction is shown in orange.

As the model provides average contents per grid cell we divide them by the cloud (resp. precipitation) fraction to obtain in-cloud contents, as it better corresponds to locally measured quantities.

LMDZ does not strictly computes and provides the mass (water content) of snow and rain but fluxes of precipitation (Madeleine et al., 2020). An estimation of the mass content from the flux is retrieved by assuming a constant fall velocity of 5 and 1 m s^{-1} for rain and snow respectively.

3.2. Spatial Co-Location of Aircraft Observations and Model Cloud Fields

To properly compare aircraft observations with model cloud fields at a given location and time, a robust method for which each observation point is as representative as possible of the model grid cell is needed. The frontal clouds sampled during the campaign generally have a typical size of a few tens of km. When the aircraft trajectory is located at the boundary between two grid cells, the question of which model grid cell to compare with—or how to interpolate model outputs—emerges. To avoid any ambiguity in the choice of the grid cell and to avoid any smoothing effect induced by interpolation, we define a "gray zone" around the perimeter of each grid cell (Figure 4): Observations located in this gray zone are discarded as neither interpolation nor nearest point is really appropriate. For the observations outside the gray zone, we select the nearest point in the model. Observations corresponding to the same grid cell are averaged and the standard deviation is computed to characterize the in-cell variability. To keep only statistics representative of the grid cell area, only grid cells with at least 100 in situ observations are kept. As the in situ probes sampling time step is 1 s and the aircraft speed is 100 m s^{-1}, this means that the aircraft flew at least 10 km inside the grid cell area.

As it is selective, this methodology discards many observations. To visually compare the continuous time evolution of the vertical cloud structure—with time-height plots—we therefore follow a less restrictive approach that guarantees continuity and visual consistency in the time series which means that at least one model grid cell is always associated with some observations. For this purpose we select the grid points located within a disk of 35-km diameter around the aircraft and average them. As the speed of the ATR42 aircraft is 100 m s^{-1}, the horizontal resolution of 27 km is equivalent to a temporal resolution of 270 s. The observations are thus averaged over intervals of 270 s to get the same horizontal resolution as the model outputs.

In both cases, the observations are compared with the nearest corresponding hourly model output.

4. Results

4.1. Case Study on Flight 40

We first illustrate the application of our comparison methodology and carry out the model evaluation on a case study which corresponds to the flight 40. This flight is deemed particularly interesting since it sampled a well-defined frontal deep cloud band surrounded by mid-level MPCs.

4.1.1. Synoptic Overview

At 12 UTC on 6 August 2022, a moderate cyclone reached a minimum sea level pressure of 1,000 hPa (see contours in Figure 5a) southeast of Svalbard and was interacting with an upper-level cold anomaly slightly upstream of its location (shadings). The cyclone was initiated over the northwestern coast of Norway at roughly 00 UTC 5 August (not shown). Associated with this cyclone are low-level clouds located north west of the pressure minimum along the warm front and mid- to high-level clouds setting north of the upper-level cold anomaly (Figures 5a and 5b). It is worth mentioning that those frontal mid- to high-level clouds were the focus and target of the flight 40. Without nudging inside the domain, ICOLMDZ reproduces a sea-level pressure field whose minimum intensity is close to that of ERA5 but the cyclone is located slightly westward of its ERA5 position (Figures 5a and 5c). There are also noticeable differences in the relative position of the surface cyclone with the upper-level cold anomaly between the model simulation and ERA5 (Figures 5b and 5d). Despite these differences in the structure and location of the surface cyclone, the frontal mid- to high-level cloud band is roughly located in the same area in the model run as in ERA5 (see red contours in Figures 5b and 5d). When nudging the wind field, the sea-level pressure as well as the warm and cold anomalies in the potential temperature fields at 850 and 500 hPa are very close to those in ERA5 (Figures 5e and 5f). The mid-level frontal cloud band is also more continuous and extends more to the east than in the simulation without nudging (Figure 5f).

Note that the aircraft trajectory passes through the whole diversity of clouds north of the cyclone ranging from high- to low-level clouds (Figures 5e and 5f).

4.1.2. Cloud Macrophysical Vertical Structure

Figure 6 compares the cloud fraction in the simulations with the cloud mask from the radar. The radar cloud mask (red contours) shows that the aircraft first passes above a cloud column at 11.25 UTC associated with the warm front and then enters a band of mid-level clouds. It crosses a deep nimbostratus cloud extending from 350 hPa down to the surface and then, while moving south, it goes through clouds with a decreasing top altitude down to around 600 hPa. Those clouds are sampled 4 times, as the aircraft goes back and forth at different altitudes. For instance, the deep nimbostratus cloud was sampled at 11.5, 12.2, and 13.3 UTC. The first three crossings of that cloud happened when the aircraft flew over the same leg at constant longitude (29°E) but different levels and then during its return leg to Svalbard (Figure 6d). The aircraft then sampled a low cloud at the end of the flight, above the coasts of Svalbard.

In ERA5 (Figure 6a), the height of the clouds is overall well represented, but their spatio-temporal location, particularly that of the nimbostratus, does not coincide with the observations. In terms of cloud macrophysical vertical structure, ERA5 biases are different from those of LMDZ, but the general pattern is not necessarily better.

In the CM7dev run (Figure 6b), the overall width and height of the deep cloud band crossed 4 times by the aircraft are rather well represented in comparison with both ERA5 and the radar mask. However, significant discrepancies are noticed: there are rather high clouds in the CM7dev run located between 400 and 600 hPa that do not appear in ERA5 or in the radar mask for instance between 11.0 and 11.3 UTC or between 12.2 and 12.7 UTC. Other differences appear in the cloud top height of the lower clouds located on both sides of the deep cloud band. In the CM7dev run, the cloud top heights are near 800 hPa while in ERA5 near 700 hPa and in the radar mask closer to 600 hPa. In brief, the CM7dev run simulates too much high cloud and too low mid-level clouds. Nudging the wind toward ERA5 within the domain (Figure 6c) helps solving the two latter points: the nimbostratus clouds are better defined albeit still too wide at the top and the lower mid-level frontal clouds reach the altitude of the observed clouds. Although nudging the wind precludes a proper analysis of the cloud-dynamics interactions, it substantially improves the spatio-temporal coincidence of the cloud structures between the model simulations and the observations as the domain is sufficiently large to make the unconstrained synoptic model fields slightly drifted from ERA5.

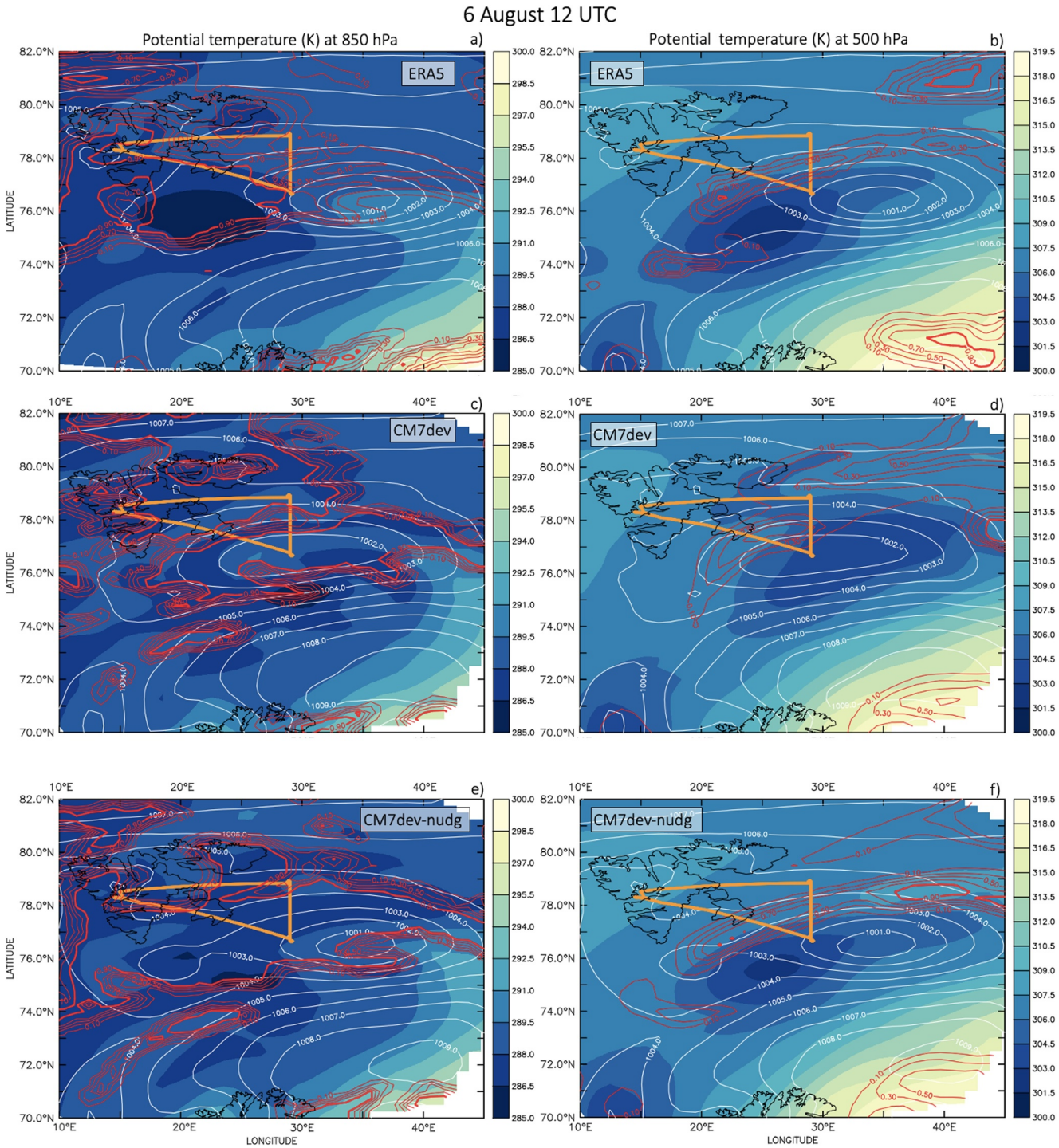

Figure 5. Left: Potential temperature (shading) and cloud fraction (red contours) at 850 hPa and mean sea level pressure (white contours) for (a) ERA5 (c) CM7dev simulation (e) CM7dev-nudg simulation Right: Potential temperature (shading) and cloud fraction (red contours) at 500 hPa (b) ERA5 (d) CM7dev simulation (f) CM7dev-nudg simulation. The domain shown ranges are 10°E–45°E and 70°N–82°N. The flight 40 trajectory is shown in orange.

As the combination of CM7dev physics with nudging in wind gives the best spatio-temporal coincidence of cloud structures in the model with respect to observations, we will use the CM7dev-nudg simulation in the following to evaluate the in-cloud water contents.

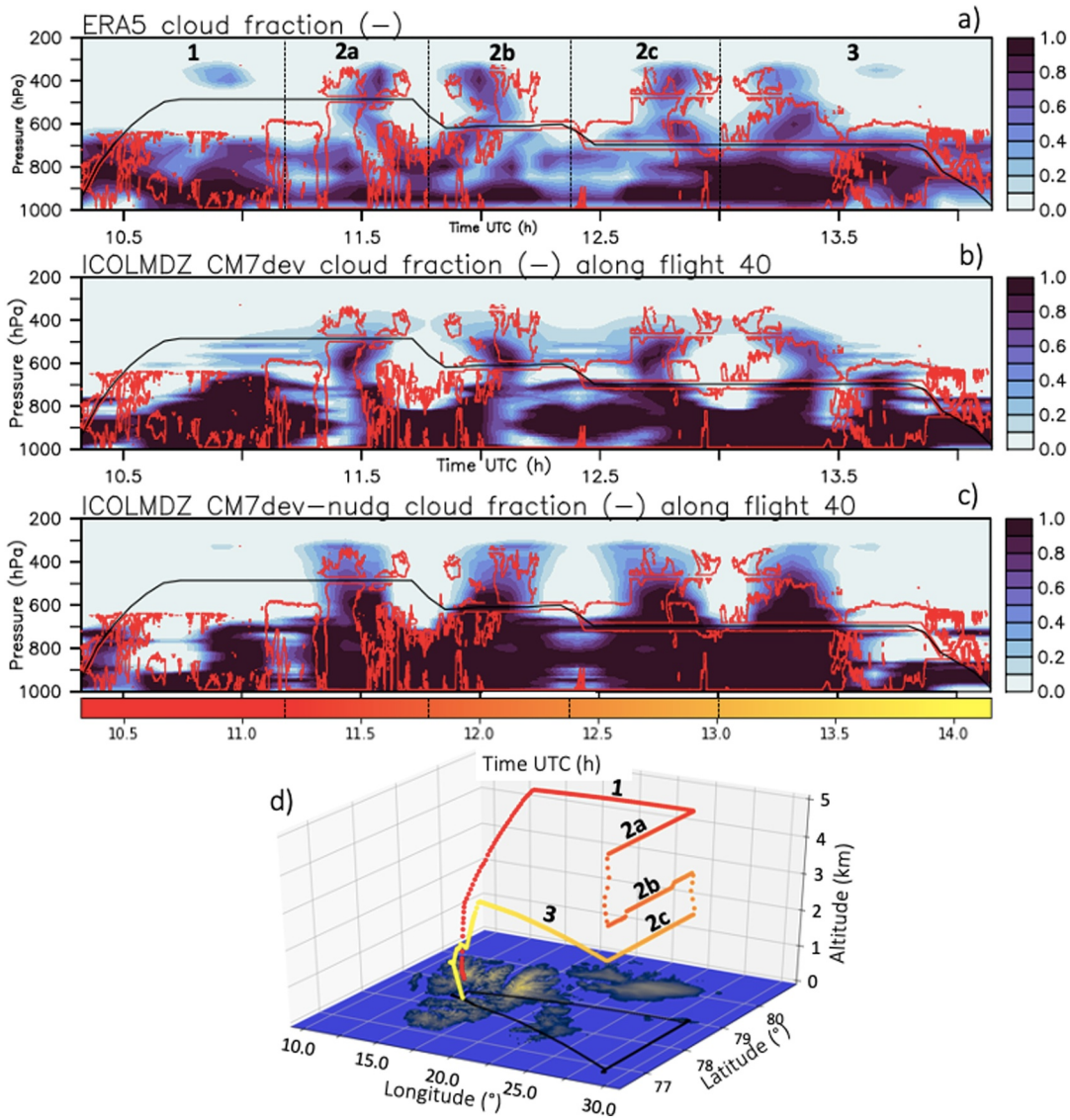

Figure 6. (a–d): Time-pressure plot along flight path for (a) ERA5 (b) CM7dev run (c) CM7dev-nudged run. Simulated cloud fraction is in color shading, cloud mask from radar is in red contours, plane location in solid black line. The location of the aircraft at each time of the x-axis of panel (a)–(c) is shown in panel (d).

4.1.3. Liquid and Ice Water Contents

Prior to using in situ merged 2D-S—HVPS measurements and radar estimates of IWC, it is worth recalling that the two independent products are consistent with each other during the whole campaign (Figure 2). For the flight 40 (Figure 7a), one can point out a slight overestimation of the radar estimation with respect to the in situ data inside the frontal cloud that is, between 12:30 and 13:30 UTC. The higher IWC values, of by 0.06–0.1 g m^{-3}, are found in the core of the nimbostratus cloud and correspond to snowfall occurrences.

ICOLMDZ (Figure 7b) generally overestimates the IWC compared to radar and in situ measurements. The explanation for this overestimation is twofold: (a) an overall excessive simulated ice amount and (b) a location of the deep snowfall core (orange shading in Figures 7a and 7b) located slightly too much to the south and a nimbostratus cloud too wide compared to observations. Looking more into details, a pattern emerges when conditioning the comparison with probe measurements to the distance from cloud top (Figure 8a). Close to cloud top the IWC is largely overestimated, and the lower the content, the greater the overestimation. Conversely, far from cloud top (>2 km) that is, in snowfall regions, the overestimation is less pronounced.

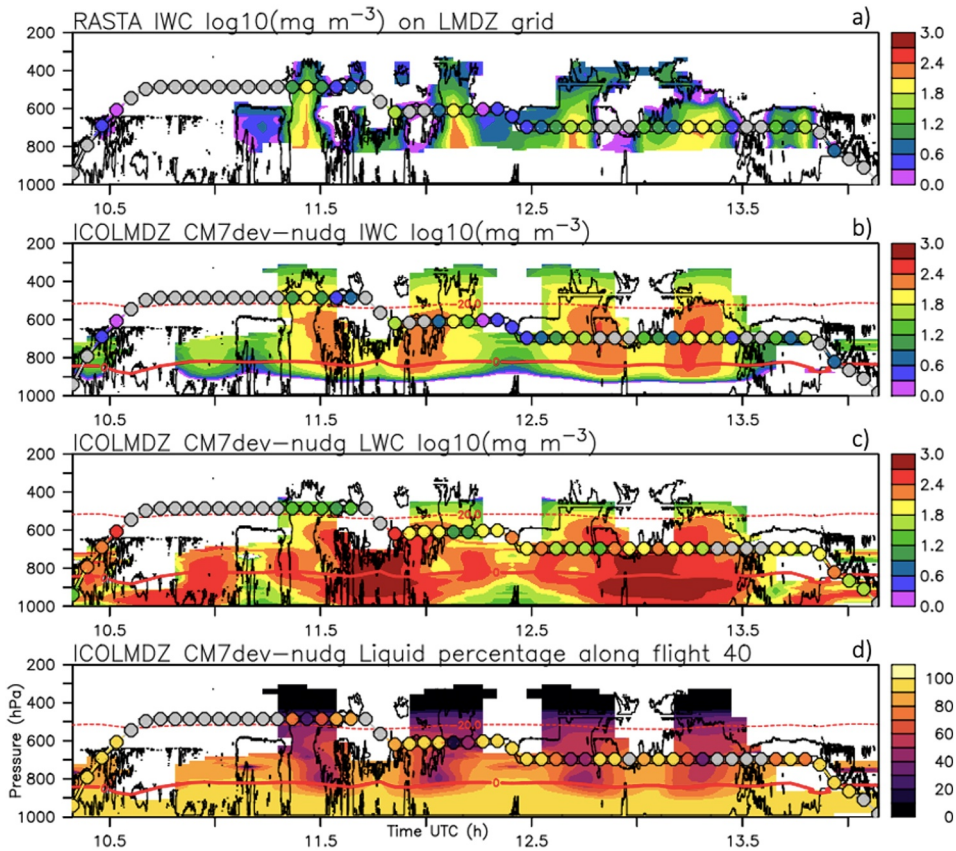

Figure 7. Time-pressure plot along flight path. (a) Retrieved IWC from the radar interpolated onto the model grid, (b) simulated IWC (c) simulated LWC (d) simulated liquid ratio. Colored circles are the corresponding quantities estimated from the HVPS (IWC) and CDP (LWC) measurements. Black contours: radar cloud mask. Red lines are isotherm 0°C (solid) and −20°C (dashed).

No ice is observed with the radar below 800 hPa which roughly corresponds to the altitude of the upper boundary of the melting layer (Figure 7a). In the model, ice is simulated down to about 900 hPa that is, nearly 100 hPa below the 0°C-isotherm (Figure 7b). The simulated melting layer is therefore around 1,000 m thick while in radar

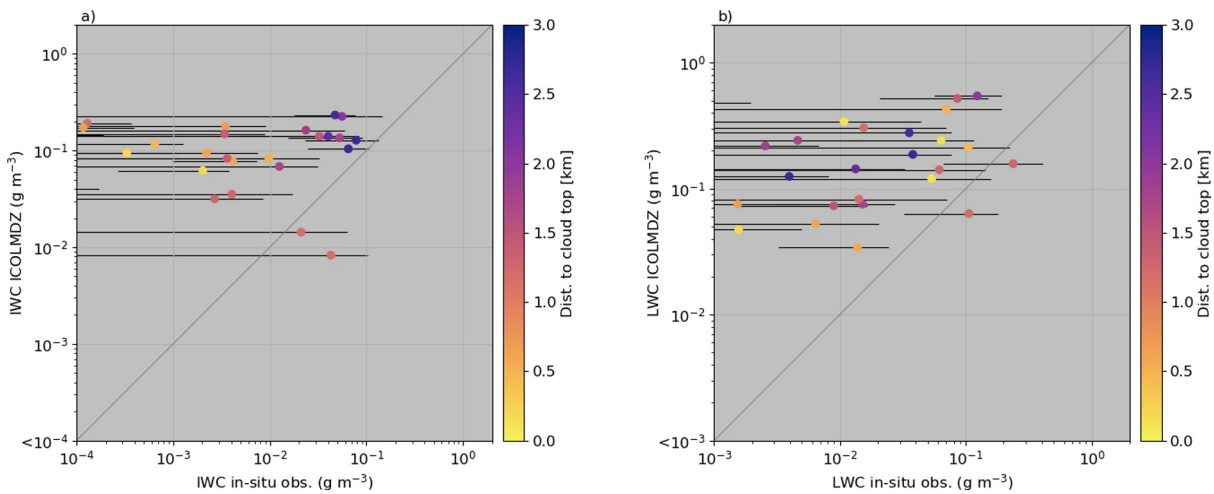

Figure 8. Scatter plots of in situ observed versus simulated (a) ice water content (IWC) and (b) liquid water content (LWC). The color refers to the distance between the altitude of the aircraft and cloud top as detected by the radar. The horizontal black lines show ± the standard deviation of observations within the corresponding grid box.

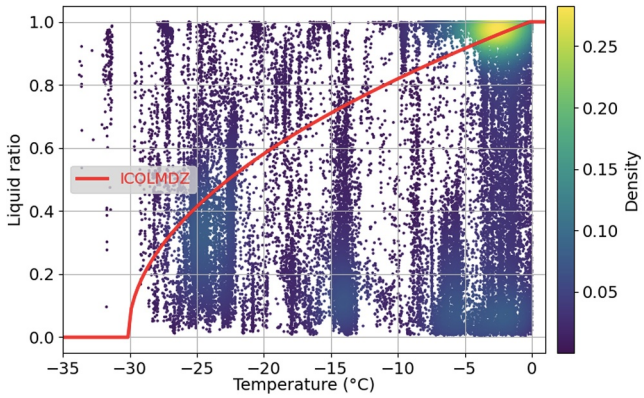

Figure 9. Scatter plot of cloud liquid ratio (LWC/(IWC + LWC)) as a function of temperature for the in situ measurements (color shading indicates the density of points) and function used for cloud phase partitioning in ICOLMDZ (red curve).

observations it is between 200 and 400 m (not shown). This raises a likely shortcoming in the parameterization of snowfall melting in the LMDZ cloud scheme.

Alike IWC, LWC is overestimated throughout the flight compared to in situ measurements (Figure 7c). The higher simulated LWC values, which corresponds to the higher overestimation as well, are found in the mid-level frontal clouds. They reach 1 g m^{-3} in LMDZ compared to a maximum of 0.2 g m^{-3} in in situ measurements. Figure 8b confirms the almost systematic overestimation of the LWC and shows it is independent upon the distance to cloud top for that flight.

In addition to the LWC and IWC overestimations, the model generally fails to represent the proportion of liquid fraction in clouds. The variations of liquid percentage measured by the probes is not correlated with the temperature variations and high liquid percentage are often observed near cloud tops. For example, between 13:30 and 13:45 the altitude of measurement and the temperature are constant but the liquid percentage goes from 90% to 40%. On the contrary, the model shows a quite continuous pattern—with a downward increase—induced by the temperature-dependent phase partitioning in the cloud scheme (Figure 7d).

4.2. Statistical Comparison Over All Flights

We now want to assess to what extent the conclusions regarding the ICOLMDZ performance drawn from flight 40 can be generalized when comparing the simulation over all the 15 flights. As the amount of condensed water depends on temperature through the saturation ratio, we first check ICOLMDZ temperature. Compared to in situ aircraft measurements, the model simulates a temperature very close to that observed. Using all flights, the mean bias is 0.13 K and the Root Mean Square Error is 1.47 K. This comparison gives us confidence in the way ICOLMDZ represents the temperature field in the clouds.

In agreement with the analysis on Flight 40 (Figure 7d) in the previous section, Figure 9 shows that the observation of the cloud liquid ratio (LWC/(LWC + IWC)) during the full campaign does not correlate with temperature. The figure further clearly shows that the temperature-dependent phase partitioning such as that used in the LMDZ cloud scheme is inappropriate to properly capture the phase of Arctic MPCs, in agreement with previous literature (e.g., Forbes & Ahlgrimm, 2014).

Figure 10 is similar to Figure 8 but it contains data from all flights. The general pattern for the IWC is very similar to that observed on flight 40. Values for points located more than 2.5 km below cloud top—which are generally of the order of 0.1 g m^{-3}—are slightly overestimated by the model (Figure 10a). Smaller observed IWC values corresponding generally to points located between cloud top and 2 km below it are largely overestimated by the model. Subsequently, the range of IWC values is larger in the in situ observations than in the model which is not able to simulate low contents.

The LWC is either overestimated or missed by the model. The first case is the most frequent and while no pattern was apparent on flight 40, one emerges in Figure 10b: the highest overestimations occur far from cloud top where they can reach one order of magnitude. Close to cloud top, the overestimation is much less pronounced. In a few situations, significant liquid content is observed but not simulated: 86% of them correspond to the model missing the cloud (situations corresponding to $\alpha_c < 0.1$): those situations are not shown in Figure 10b. We only show the cases for which the model simulates a cloud but with no liquid content (triangles in Figure 10b), to highlight the phase partitioning bias. These situations correspond to simulated temperatures below −30°C, for which the phase-partitioning function in LMDZ does not allow any liquid (Madeleine et al., 2020). Tests without the gray zone and with grid-average values instead of in-cloud were also performed (not shown). The results obtained from the different tests are overall very close, which confirm the robustness of the above conclusions with respect to our methodological choice.

To complement and strengthen the evaluation of the simulated IWC, we now use radar IWC estimates which provide information on the vertical distribution of ice condensates. Figure 11a shows that the 2D joint distribution

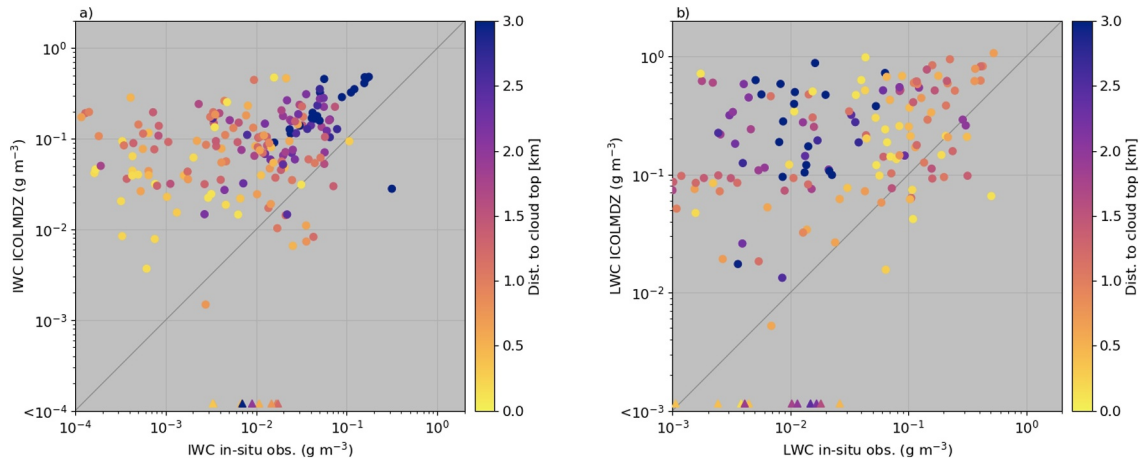

Figure 10. Same as Figure 8 but using data from all the flights. Triangles correspond to points with a cloud fraction $\alpha_c > 0.1$ and IWC $< 10^{-4}$ g m^{-3} (resp. LWC $< 10^{-3}$ g m^{-3}) in the model. They have been (artificially) plotted at the very bottom of the graph to make them visible.

of the IWC observed by the radar exhibits 2 modes: the main mode corresponds to ice precipitation growing as it falls down from the high troposphere within deep nimbostratus clouds. The second mode corresponds to lower and relatively constant IWC values between 6 and 2 km of about $\approx 10^{-3}$ g m^{-3}, and rather correspond to mid-levels clouds surrounding the deep precipitating system such as altostratus and altocumulus clouds. Such a bimodality is also noticeable in the 2D-joint distribution of the snow precipitation flux in Figure 12a. The bimodality is not simulated by the model for both the IWC (Figure 11b) and the snow precipitation flux (Figure 12b). ICOLMDZ reproduces only the main mode even if we exclude the snowfall mass from the IWC (Figure 11c). In both panels b and c of Figure 11, IWC is overestimated above 4 km and above 3 km, the "slope" of the data along the vertical is absent in the model distributions suggesting that ice crystals do no significantly grow

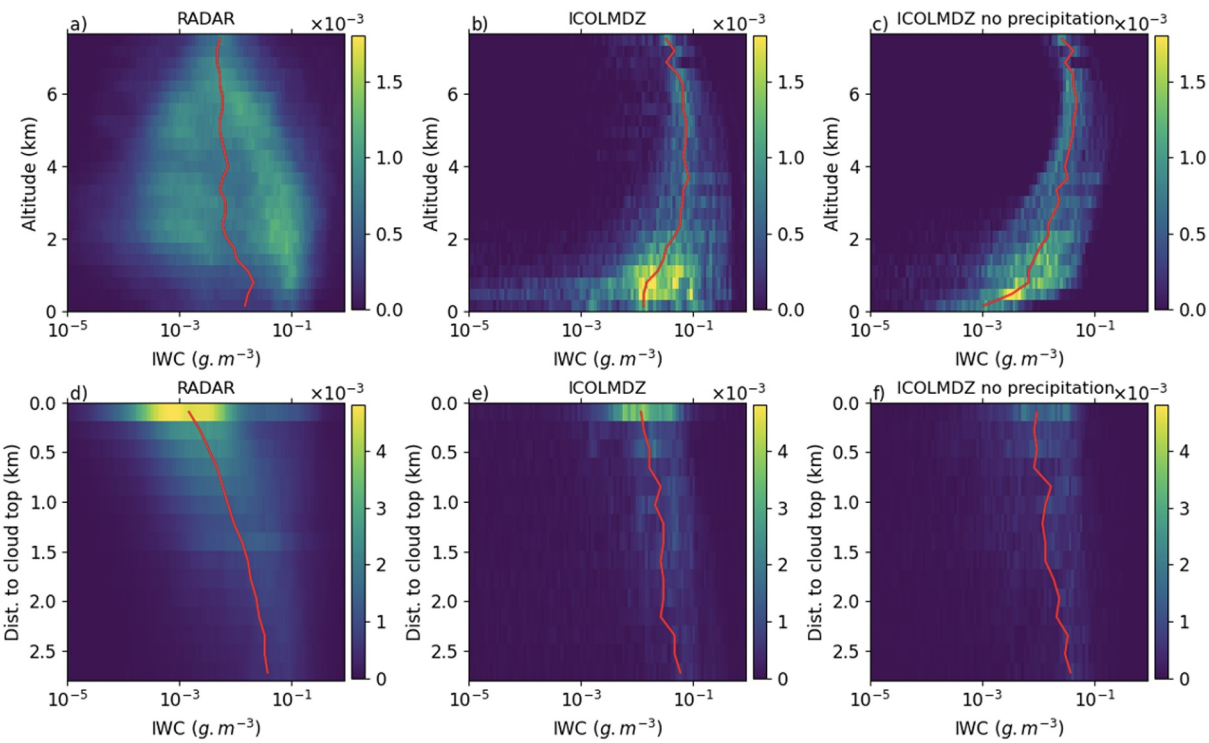

Figure 11. 2D joint distribution of ice water content as a function of altitude (a–c) and distance to cloud top (d–f) for radar observations (a and d), ICOLMDZ including the mass of snow precipitation (b and e) and ICOLMDZ without snow precipitation (c and f). The red line is the median IWC of the distribution for each altitude bin.

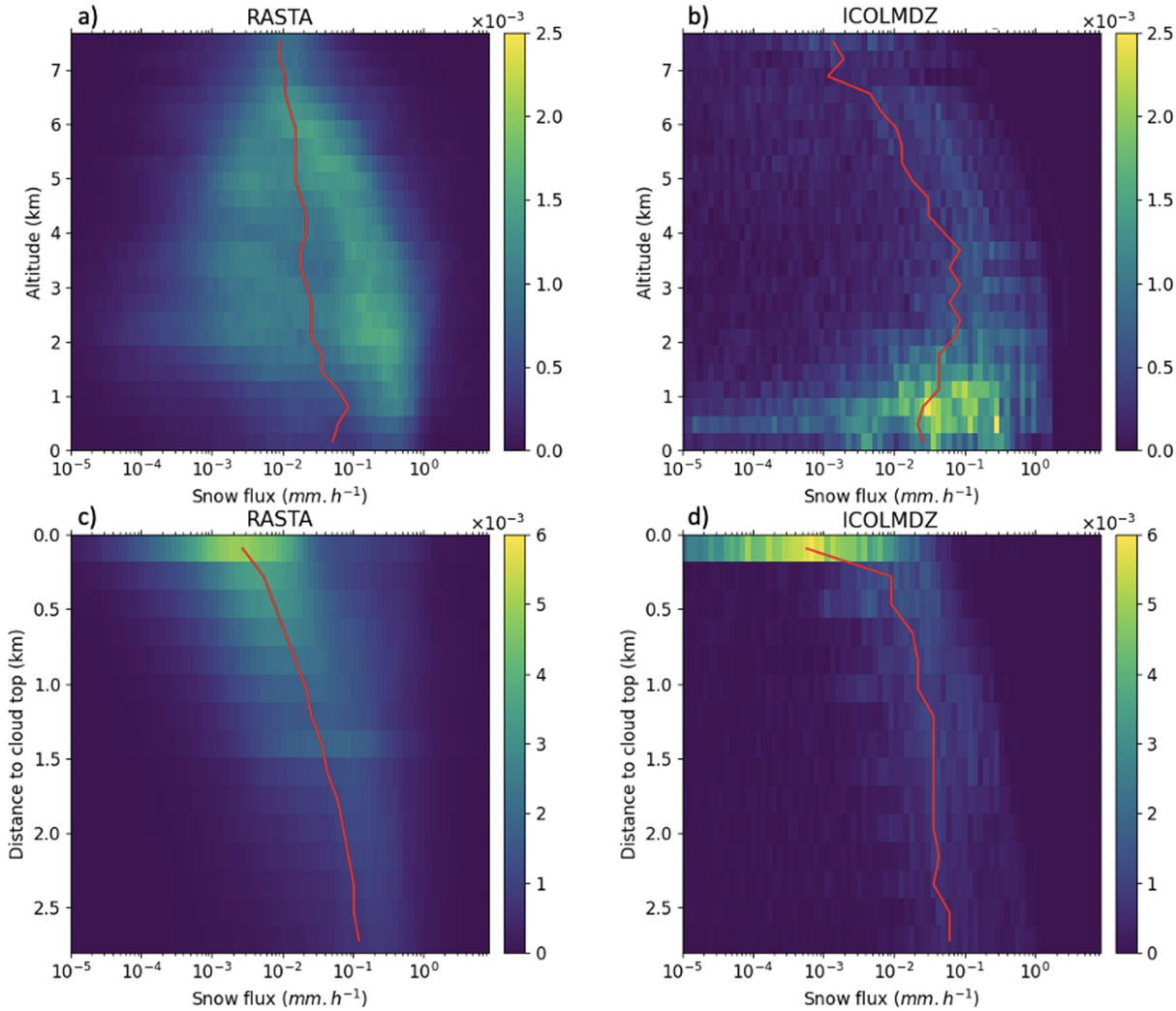

Figure 12. 2D joint distribution of snow flux as a function of altitude (a, b) and distance to cloud top (c, d) for radar observations (a and c) and ICOLMDZ (b and d). The red line is the median IWC of the distribution for each altitude bin.

as they fall in the model. It is also worth noting that the model simulates too frequent low IWC values and snowfall flux below 1 km down to the ground surface (Figures 11b and 12b). This echoes conclusions drawn from Figure 7b questioning the way the LMDZ cloud scheme represent snowfall melting, sometimes leaving unrealistic weak snow contents well below the melting layer.

The distributions of IWC as a function of the distance to cloud top (Figures 11d–11f) concurs with the agreement between observed and simulated IWC further than ∼2 km from cloud top—and the overestimation above—noticed in Figure 10a. Observed contents are the most often comprised between 10^{-3} and 10^{-2} g m^{-3} whereas they generally range between 10^{-2} and 10^{-1} g m^{-3} in the model. As the IWC does not grow downward, little or no ice precipitation growth is noticeable in the model down to 1.5 km below cloud top (Figure 12d), whereas the observed ice precipitation distribution exhibits a clear slope (Figure 12c). The 2D joint distributions of IWC (Figures 11 and 12) remain unchanged when using the CM7dev simulation (i.e., the simulation without nudging in wind inside the domain) (not shown), meaning that the statistical relationships observed are independent of where and when the clouds occur in the model, which concur with the conclusions of D'Alessandro et al. (2019).

Overall, it is worth emphasizing that despite uncertainties associated with the IWC retrieval from the radar, the conclusions regarding the simulated IWC evaluation using the two independent in situ and radar data sets are consistent.

5. Summary and Conclusions

By using airborne measurements from a Doppler radar and microphysical probes obtained during the RALI-THINICE campaign, we have assessed the representation of clouds associated with Arctic cyclones in the ICOLMDZ model. We conducted two simulations—one with nudging of the wind inside the domain, one without—with the new Limited Area Model configuration of ICOLMDZ on a domain with a horizontal resolution of 27.5 km. Nudging the wind inside the simulation domain toward ERA5 improves the spatio-temporal coincidence of cloud structures in the model with respect to observations. The simulation with nudging was thus retained for the in-cloud water contents evaluation even though feedbacks from clouds onto the cyclone dynamics are thereby precluded. We then developed a methodology to compute observational quantities that can be reliably compared to mesh-averaged simulated variables. Airborne radar and microphysical probes products were then used to evaluate the simulated clouds in terms of ice and liquid in-cloud contents with a specific attention on the vertical distribution of the phase.

From those comparisons, we identified several major shortcomings in the simulation. Close to clouds tops, the model produces an overly high IWC and slightly too much cloud liquid water. Moreover, a sharp increase in snowfall flux is simulated just below cloud top while radar data suggest a more gradual growth of precipitation. Conversely, far from cloud tops supercooled LWC is highly overestimated and the IWC is slightly overestimated. The snowfall flux is fairly well represented far from cloud tops but significant low snowfall values unrealistically remains at low-levels, well below the melting layer. It is worth noting that the overestimation of LWC in mid-level clouds by LMDZ concurs with the conclusions of Flack et al. (2021) for cases of extratropical cyclones above the Atlantic Ocean. Overall, we can conclude that the temperature-dependent phase partitioning parameterization in the LMDZ cloud scheme (Madeleine et al., 2020) is inappropriate to properly simulate Arctic MPCs, concurring with previous studies using other models (e.g., Forbes & Ahlgrimm, 2014). A possible follow-up of this work could be to advance this phase partitioning in LMDZ and make it dependent on the turbulent activity and aerosols properties following Field et al. (2014) and Furtado et al. (2016). One could hence leverage the lidar data collected during RALI-THINICE to identify the supercooled liquid layers as well as the Doppler signal of the radar to derive information on the turbulence. Moreover, the present study highlighted the poor vertical evolution of ice precipitation in LMDZ, inviting for further improvements of the parameterizations of the autoconversion process, snowflake growth and melting.

Data Availability Statement

RALI-THINICE data are freely distributed on the campaign website https://ralithinice.aeris-data.fr/. The LMDZ and DYNAMICO models are freely distributed at the following links https://web.lmd.jussieu.fr/~lmdz/pub/ and https://gitlab.in2p3.fr/ipsl/projets/dynamico/dynamico. The model configuration used for this study is available at the following link http://forge.ipsl.jussieu.fr/igcmg/browser/CONFIG/publications/ICOLMDZOR_LAM_modipsl_rev6422_2023.

Acknowledgments
This project has been financed by the CNRS-INSU LEFE-EC2CO CYCLONICE project. Simulations were performed using HPC resources from the IDRIS (Institut du Développement et des Ressources en Informatique Scientifique, CNRS, France), projects WUU ADA0110111116. Airborne data were obtained using the aircraft managed by SAFIRE, the French facility for airborne research, an infrastructure of the French National Center for Scientific Research (CNRS), Météo-France and the French National Center for Space Studies (CNES). Most of the microphysical in situ data were collected using instruments (CDP-2, 2D-S, PIP, HVPS, CVI-snow, ROBUST) from the French Airborne Measurement Platform, a facility partially funded by CNRS/INSU and CNES. The processing of microphysical data have been supported by the EECLAT project, funded by CNES. We also acknowledge support from the DEPHY research group, funded by CNRS/INSU and Météo-France.

References

Barrett, A. I., Hogan, R. J., & Forbes, R. M. (2017). Why are mixed-phase altocumulus clouds poorly predicted by large-scale models? Part 2. Vertical resolution sensitivity and parameterization. *Journal of Geophysical Research: Atmospheres*, *122*(18), 9927–9944. https://doi.org/10.1002/2016jd026322

Barrett, P. A., Blyth, A., Brown, P. R., & Abel, S. J. (2020). The structure of turbulence and mixed-phase cloud microphysics in a highly supercooled altocumulus cloud. *Atmospheric Chemistry and Physics*, *20*(4), 1921–1939. https://doi.org/10.5194/acp-20-1921-2020

Boucher, O., Servonnat, J., Albright, A. L., Aumont, O., Balkanski, Y., Bastrikov, V., et al. (2020). Presentation and evaluation of the IPSL-CM6A-LR climate model. *Journal of Advances in Modeling Earth Systems*, *12*(7), e2019MS002010. https://doi.org/10.1029/2019ms002010

Bourdin, S., Fromang, S., Caubel, A., Ghattas, J., Meurdesoif, Y., & Dubos, T. (2023). Tropical cyclones in global high-resolution simulations using the IPSL model.

Cesana, G., Waliser, D., Jiang, X., & Li, J.-L. (2015). Multimodel evaluation of cloud phase transition using satellite and reanalysis data. *Journal of Geophysical Research: Atmospheres*, *120*(15), 7871–7892. https://doi.org/10.1002/2014jd022932

Cheruy, F., Ducharne, A., Hourdin, F., Musat, I., Vignon, É., Gastineau, G., et al. (2020). Improved near-surface continental climate in IPSL-CM6A-LR by combined evolutions of atmospheric and land surface physics. *Journal of Advances in Modeling Earth Systems*, *12*(10), e2019MS002005. https://doi.org/10.1029/2019ms002005

Conesa, P. (2022). Climate simulations with the limited-area model DYNAMICO-LMDZ (Master's Thesis). (In french).

Crosier, J., Bower, K., Choularton, T., Westbrook, C. D., Connolly, P., Cui, Z., et al. (2011). Observations of ice multiplication in a weakly convective cell embedded in supercooled mid-level stratus. *Atmospheric Chemistry and Physics*, *11*(1), 257–273. https://doi.org/10.5194/acp-11-257-2011

D'Alessandro, J. J., Diao, M., Wu, C., Liu, X., Jensen, J. B., & Stephens, B. B. (2019). Cloud phase and relative humidity distributions over the southern ocean in austral summer based on in situ observations and CAM5 simulations. *Journal of Climate*, *32*(10), 2781–2805. https://doi.org/10.1175/jcli-d-18-0232.1

Delanoë, J., Heymsfield, A. J., Protat, A., Bansemer, A., & Hogan, R. J. (2014). Normalized particle size distribution for remote sensing application. *Journal of Geophysical Research: Atmospheres*, *119*(7), 4204–4227. https://doi.org/10.1002/2013JD020700

Delanoë, J., & Hogan, R. J. (2008). A variational scheme for retrieving ice cloud properties from combined radar, lidar, and infrared radiometer. *Journal of Geophysical Research*, *113*(D7), D07204. https://doi.org/10.1029/2007jd009000

Delanoë, J., Protat, A., Bouniol, D., Heymsfield, A., Bansemer, A., & Brown, P. (2007). The characterization of ice cloud properties from Doppler radar measurements. *Journal of Applied Meteorology and Climatology*, *46*(10), 1682–1698. https://doi.org/10.1175/jam2543.1

Delanoë, J., Protat, A., Jourdan, O., Pelon, J., Papazzoni, M., Dupuy, R., et al. (2013). Comparison of airborne in situ, airborne radar–lidar, and spaceborne radar–lidar retrievals of polar ice cloud properties sampled during the POLARCAT campaign. *Journal of Atmospheric and Oceanic Technology*, *30*(1), 57–73. https://doi.org/10.1175/JTECH-D-11-00200.1

Dubos, T., Dubey, S., Tort, M., Mittal, R., Meurdesoif, Y., & Hourdin, F. (2015). DYNAMICO-1.0, an icosahedral hydrostatic dynamical core designed for consistency and versatility. *Geoscientific Model Development*, *8*(10), 3131–3150. https://doi.org/10.5194/gmd-8-3131-2015

Dupuy, R., Jourdan, O., Mioche, G., Ehrlich, A., Waitz, F., Gourbeyre, C., et al. (2018). Cloud microphysical properties of summertime Arctic stratocumulus during the ACLOUD campaign: Comparison with previous results in the European Arctic. In *15th conference on cloud physics*.

Field, P., Hill, A., Furtado, K., & Korolev, A. (2014). Mixed-phase clouds in a turbulent environment. Part 2: Analytic treatment. *Quarterly Journal of the Royal Meteorological Society*, *140*(680), 870–880. https://doi.org/10.1002/qj.2175

Flack, D. L., Rivière, G., Musat, I., Roehrig, R., Bony, S., Delanoë, J., et al. (2021). Representation by two climate models of the dynamical and diabatic processes involved in the development of an explosively deepening cyclone during NAWDEX. *Weather and Climate Dynamics*, *2*(1), 233–253. https://doi.org/10.5194/wcd-2-233-2021

Forbes, R. M., & Ahlgrimm, M. (2014). On the representation of high-latitude boundary layer mixed-phase cloud in the ECMWF global model. *Monthly Weather Review*, *142*(9), 3425–3445. https://doi.org/10.1175/mwr-d-13-00325.1

Fridlind, A. M., & Ackerman, A. S. (2018). Simulations of Arctic mixed-phase boundary layer clouds: Advances in understanding and outstanding questions. *Mixed-Phase Clouds*, 153–183. https://doi.org/10.1016/b978-0-12-810549-8.00007-6

Furtado, K., Field, P., Boutle, I., Morcrette, C., & Wilkinson, J. (2016). A physically based subgrid parameterization for the production and maintenance of mixed-phase clouds in a general circulation model. *Journal of the Atmospheric Sciences*, *73*(1), 279–291. https://doi.org/10.1175/jas-d-15-0021.1

Hersbach, H., Bell, B., Berrisford, P., Hirahara, S., Horányi, A., Muñoz-Sabater, J., et al. (2020). The ERA5 global reanalysis. *Quarterly Journal of the Royal Meteorological Society*, *146*(730), 1999–2049. https://doi.org/10.1002/qj.3803

Hofer, S., Tedstone, A. J., Fettweis, X., & Bamber, J. L. (2019). Cloud microphysics and circulation anomalies control differences in future Greenland melt. *Nature Climate Change*, *9*(7), 523–528. https://doi.org/10.1038/s41558-019-0507-8

Hogan, R. J., Tian, L., Brown, P. R. A., Westbrook, C. D., Heymsfield, A. J., & Eastment, J. D. (2012). Radar scattering from ice aggregates using the horizontally aligned oblate spheroid approximation. *Journal of Applied Meteorology and Climatology*, *51*(3), 655–671. https://doi.org/10.1175/JAMC-D-11-074.1

Hourdin, F., Rio, C., Grandpeix, J.-Y., Madeleine, J.-B., Cheruy, F., Rochetin, N., et al. (2020). LMDZ6A: The atmospheric component of the IPSL climate model with improved and better tuned physics. *Journal of Advances in Modeling Earth Systems*, *12*(7), e2019MS001892. https://doi.org/10.1029/2019ms001892

Jakob, C., & Klein, S. A. (2000). A parametrization of the effects of cloud and precipitation overlap for use in general-circulation models. *Quarterly Journal of the Royal Meteorological Society*, *126*(568), 2525–2544. https://doi.org/10.1002/qj.49712656809

Kay, J. E., & Gettelman, A. (2009). Cloud influence on and response to seasonal Arctic sea ice loss. *Journal of Geophysical Research*, *114*(D18), D18204. https://doi.org/10.1029/2009jd011773

Kay, J. E., L'Ecuyer, T., Chepfer, H., Loeb, N., Morrison, A., & Cesana, G. (2016). Recent advances in Arctic cloud and climate research. *Current Climate Change Reports*, *2*(4), 159–169. https://doi.org/10.1007/s40641-016-0051-9

Klein, S. A., McCoy, R. B., Morrison, H., Ackerman, A. S., Avramov, A., Boer, G. D., et al. (2009). Intercomparison of model simulations of mixed-phase clouds observed during the ARM mixed-phase Arctic cloud experiment. I: Single-layer cloud. *Quarterly Journal of the Royal Meteorological Society: A Journal of the Atmospheric Sciences, Applied Meteorology and Physical Oceanography*, *135*(641), 979–1002. https://doi.org/10.1002/qj.416

Komurcu, M., Storelvmo, T., Tan, I., Lohmann, U., Yun, Y., Penner, J. E., et al. (2014). Intercomparison of the cloud water phase among global climate models. *Journal of Geophysical Research: Atmospheres*, *119*(6), 3372–3400. https://doi.org/10.1002/2013jd021119

Korolev, A., & Milbrandt, J. (2022). How are mixed-phase clouds mixed? *Geophysical Research Letters*, *49*(18), e2022GL099578. https://doi.org/10.1029/2022gl099578

Lackner, C. P., Geerts, B., Juliano, T. W., Xue, L., & Kosovic, B. (2023). Vertical structure of clouds and precipitation during Arctic cold-air outbreaks and warm-air intrusions: Observations from COMBLE. *Journal of Geophysical Research: Atmospheres*, *128*(13), e2022JD038403. https://doi.org/10.1029/2022jd038403

Lance, S., Brock, C., Rogers, D., & Gordon, J. (2010). Water droplet calibration of the cloud droplet probe (CDP) and in-flight performance in liquid, ice and mixed-phase clouds during ARCPAC. *Atmospheric Measurement Techniques*, *3*(6), 1683–1706. https://doi.org/10.5194/amt-3-1683-2010

Lawson, R. P., O'Connor, D., Zmarzly, P., Weaver, K., Baker, B., Mo, Q., & Jonsson, H. (2006). The 2D-S (stereo) probe: Design and preliminary tests of a new airborne, high-speed, high-resolution particle imaging probe. *Journal of Atmospheric and Oceanic Technology*, *23*(11), 1462–1477. https://doi.org/10.1175/jtech1927.1

Lawson, R. P., Stewart, R. E., Strapp, J. W., & Isaac, G. A. (1993). Aircraft observations of the origin and growth of very large snowflakes. *Geophysical Research Letters*, *20*(1), 53–56. https://doi.org/10.1029/92gl02917

Lenaerts, J., Camron, M. D., Wyburn-Powell, C. R., & Kay, J. E. (2020). Present-day and future Greenland ice sheet precipitation frequency from CloudSat observations and the community Earth system model. *The Cryosphere*, *14*(7), 2253–2265. https://doi.org/10.5194/tc-14-2253-2020

Lenaerts, J. T., Van Tricht, K., Lhermitte, S., & L'Ecuyer, T. S. (2017). Polar clouds and radiation in satellite observations, reanalyses, and climate models. *Geophysical Research Letters*, *44*(7), 3355–3364. https://doi.org/10.1002/2016gl072242

Listowski, C., & Lachlan-Cope, T. (2017). The microphysics of clouds over the Antarctic Peninsula–part 2: Modelling aspects within polar WRF. *Atmospheric Chemistry and Physics*, *17*(17), 10195–10221. https://doi.org/10.5194/acp-17-10195-2017

Madeleine, J.-B., Hourdin, F., Grandpeix, J.-Y., Rio, C., Dufresne, J.-L., Vignon, E., et al. (2020). Improved representation of clouds in the atmospheric component LMDZ6A of the IPSL-CM6A Earth system model. *Journal of Advances in Modeling Earth Systems*, *12*(10), e2020MS002046. https://doi.org/10.1029/2020ms002046

McCusker, G. Y., Vüllers, J., Achtert, P., Field, P., Day, J. J., Forbes, R., et al. (2023). Evaluating Arctic clouds modelled with the unified model and integrated forecasting system. *Atmospheric Chemistry and Physics*, *23*(8), 4819–4847. https://doi.org/10.5194/acp-23-4819-2023

McIlhattan, E. A., L'Ecuyer, T. S., & Miller, N. B. (2017). Observational evidence linking Arctic supercooled liquid cloud biases in CESM to snowfall processes. *Journal of Climate*, *30*(12), 4477–4495. https://doi.org/10.1175/jcli-d-16-0666.1

Mioche, G., Jourdan, O., Ceccaldi, M., & Delanoë, J. (2015). Variability of mixed-phase clouds in the Arctic with a focus on the Svalbard region: A study based on spaceborne active remote sensing. *Atmospheric Chemistry and Physics*, *15*(5), 2445–2461. https://doi.org/10.5194/acp-15-2445-2015

Morrison, H., De Boer, G., Feingold, G., Harrington, J., Shupe, M. D., & Sulia, K. (2012). Resilience of persistent Arctic mixed-phase clouds. *Nature Geoscience*, *5*(1), 11–17. https://doi.org/10.1038/ngeo1332

Morrison, H., McCoy, R. B., Klein, S. A., Xie, S., Luo, Y., Avramov, A., et al. (2009). Intercomparison of model simulations of mixed-phase clouds observed during the ARM mixed-phase Arctic cloud experiment. II: Multilayer cloud. *Quarterly Journal of the Royal Meteorological Society: A Journal of the Atmospheric Sciences, Applied Meteorology and Physical Oceanography*, *135*(641), 1003–1019. https://doi.org/10.1002/qj.415

Moser, M., Voigt, C., Jurkat-Witschas, T., Hahn, V., Mioche, G., Jourdan, O., et al. (2023). Microphysical and thermodynamic phase analyses of Arctic low-level clouds measured above the sea ice and the open ocean in spring and summer. *Atmospheric Chemistry and Physics Discussions*, *23*(13), 1–27. https://doi.org/10.5194/acp-23-7257-2023

Rotstayn, L. D., Ryan, B. F., & Katzfey, J. J. (2000). A scheme for calculation of the liquid fraction in mixed-phase stratiform clouds in large-scale models. *Monthly Weather Review*, *128*(4), 1070–1088. https://doi.org/10.1175/1520-0493(2000)128<1070:asfcot>2.0.co;2

Shupe, M. D., Rex, M., Blomquist, B., Persson, P. O. G., Schmale, J., Uttal, T., et al. (2022). Overview of the MOSAiC expedition: Atmosphere. *Elementa: Science of the Anthropocene*, *10*(1), 00060. https://doi.org/10.1525/elementa.2021.00060

Silber, I., Fridlind, A. M., Verlinde, J., Ackerman, A. S., Cesana, G. V., & Knopf, D. A. (2021). The prevalence of precipitation from polar supercooled clouds. *Atmospheric Chemistry and Physics*, *21*(5), 3949–3971. https://doi.org/10.5194/acp-21-3949-2021

Touzé-Peiffer, L. (2021). Parameterization of atmospheric convection in numerical climate models—Practices and epistemological challenges (Theses, Sorbonne Université). Retrieved from https://theses.hal.science/tel-04215936

Verlinde, J., Harrington, J. Y., McFarquhar, G., Yannuzzi, V., Avramov, A., Greenberg, S., et al. (2007). The mixed-phase Arctic cloud experiment. *Bulletin of the American Meteorological Society*, *88*(2), 205–222. https://doi.org/10.1175/bams-88-2-205

Vignon, É., Alexander, S., DeMott, P., Sotiropoulou, G., Gerber, F., Hill, T., et al. (2021). Challenging and improving the simulation of mid-level mixed-phase clouds over the high-latitude southern ocean. *Journal of Geophysical Research: Atmospheres*, *126*(7), e2020JD033490. https://doi.org/10.1029/2020jd033490

Wendisch, M., Macke, A., Ehrlich, A., Lüpkes, C., Mech, M., Chechin, D., et al. (2019). The Arctic cloud puzzle: Using ACLOUD/PASCAL multiplatform observations to unravel the role of clouds and aerosol particles in Arctic amplification. *Bulletin of the American Meteorological Society*, *100*(5), 841–871. https://doi.org/10.1175/bams-d-18-0072.1